Applied Catalysis B: Environmental 174–175 (2015) 361–366

Contents lists available at ScienceDirect

Applied Catalysis B: Environmental

journal homepage: www.elsevier.com/locate/apcatb

One-pot synthesis of small and uniform Au@PtCu core–alloy shell nanoparticles as an efficient electrocatalyst for direct methanol fuel cells

Zhi Liang Zhao[a,b], Lian Ying Zhang[a,b], Shu Juan Bao[a,b], Chang Ming Li[a,b,*]

[a] Institute for Clean Energy & Advanced Materials, Faculty of Materials and Energy, Southwest University, Chongqing 400715, PR China
[b] Chongqing Key Laboratory for Advanced Materials and Technologies of Clean Energies, Chongqing 400715, PR China

ARTICLE INFO

Article history:
Received 15 September 2014
Received in revised form 21 January 2015
Accepted 12 March 2015
Available online 14 March 2015

Keywords:
Fuel cells
Electrocatalyst
Methanol oxidation
Core–shell nanoparticles
One-pot

ABSTRACT

Metal core–shell nanostructures have been extensively studied as one of the most promising electrocatalysts to significantly reduce the loading of the expensive Pt catalyst for fuel cells but it is very challenging to fabricate such a structure to possess proper metal components while making small and uniformly distributed nanoparticles for high catalytic performance. In this work, small and uniformly distributed Au-core/PtCu alloy–shell structured nanoparticles (Au@PtCu NPs) were fabricated by a novel one-pot facile method. The as-prepared Au@PtCu/C has a much larger electrochemical active surface area (ECSA) (64.8 $m^2\ g^{-1}{}_{Pt}$) than that of AuPtCu/C(38.5 $m^2\ g^{-1}{}_{Pt}$), PtCu/C (31.02 $m^2\ g^{-1}{}_{Pt}$) and commercial Pt/C (25.4 $m^2\ g^{-1}{}_{Pt}$) catalyst. This new catalyst not only greatly reduces Pt loading but also significantly increases the catalytic activity and stability toward methanol oxidation reaction in comparison to the commercial electrocatalyst. This is mainly attributed to a synergistic effect from the small and uniform core–shell nanostructure and the unique chemical compositions of Au and PtCu alloy, thus offering a great potential for a less expensive but highly active catalyst toward direct methanol fuel cells (DMFCs).

1. Introduction

The increasing concerns over environmental pollution and growing global energy consumption have stimulated intense research on clean and efficient power sources [1–5]. DMFCs are very promising for future green energy technologies, particularly for hybrid vehicles and portable electrical sources due to their high energy density, low pollution and convenient liquid nature for easy storage and transportation [6–8]. The noble metal platinum (Pt) has long been recognized as the best catalyst toward methanol oxidation. Nevertheless, Pt catalyst suffers from sluggish kinetics, high cost, instability and easy poisoning by intermediates during operation, thus greatly impeding the commercialization of DMFCs [9–11]. Therefore, it is essential to develop an efficient Pt-less or Pt-free electrocatalyst for DMFCs. In recently years, Pt-based alloy NPs have demonstrated higher catalytic activity than plain Pt catalyst [12,13]. PtRu as one of Pt-based alloys has received much attention in methanol oxidation, in which Ru can reduce the loading of expensive Pt while increasing poison resistance of intermediates. However, Ru is also a noble metal suffering from high cost and scarce reserves. Interestingly, some non-noble metals such as Cu, Co can also alloy Pt to play the same role as Ru but they are much less expensive [14–16]. In particular, Cu is one kind of earth-abundant element and can be received easily. Further, core–shell structured NPs can enhance mass activity and stability [17–19]. Towards methanol oxidation, researches are mainly focused on Pt shell with a monometallic or bimetallic alloy core structure [20–22]. Zeng et al. [20] have reported that Au core effectively promotes the electroactivity of Pt for methanol oxidation due to improved electron transfer ability from Au to Pt and more active oxygen species on Pt. Recently a core–shell structure comprising a monometallic core and Pt based bimetallic alloy shell shows further improved catalytic activity and durability toward oxygen reduction reaction [23,24]. However, the preparation method requires complicated fabrication steps while having great difficulty to achieve small and uniform dispersion attenuating the ECSA, thus often resulting in low electrocatalytic activity. In addition, such a core–shell structure has not been investigated toward methanol oxidation.

Herein a facile one-pot approach is innovated by us to successively prepare small and uniformly dispersed Au@PtCu core–alloy shell NPs, which demonstrates the much higher catalytic activity and better stability toward methanol oxidation than that of the

* Corresponding author at: Institute for Clean Energy & Advanced Materials, Faculty of Materials and Energy, Southwest University, Chongqing 400715, PR China. Tel.: +86 23 68254969; fax: +86 23 68254969.
E-mail address: ecmli@swu.edu.cn (C.M. Li).

http://dx.doi.org/10.1016/j.apcatb.2015.03.020
0926-3373/

AuPtCu ternary alloy, PtCu, commercial Pt/C and PtRu/C electrocatalyst. This new catalyst tremendously enhances the Pt mass activity by increasing an effective Pt surface area and intrinsic catalytic activity, thus holding a great promise as an efficient low-Pt electrocatalyst for applications in DMFCs.

2. Experimental

2.1. Materials

Chloroplatinic acid hexahydrate ($H_2PtCl_6{\cdot}6H_2O$, Pt ≥ 37.5%), gold chloride trihydrate ($HAuCl_4{\cdot}4H_2O$, Au ≥ 48.0%) and oleylamine (OAm, $CH_3(CH_2)_7CH{=}CH(CH_2)_8NH_2$, 70%) were purchased from Aladdin Industrial. Copper acetylacetonate ($Cu(acac)_2$, 99.99%), methanol (CH_3OH, 99.9%), perchioric acid ($HClO_4$, 70.0%) and Nafion (5 wt%) were purchased from Sigma–Aldrich. Commercial Pt/C and PtRu/C was purchased from E-TEK and Johnson-Matthey, respectively.

2.2. Synthesis of Au@PtCu NPs

As schematically illustrated in Fig. 1, Au@PtCu core–alloy shell NPs were synthesized by one-pot sequential reductions. Typically, 0.05 mmol $HAuCl_4{\cdot}4H_2O$ were dissolved in 20 mL OAm, heated to 130 °C and then held for an hour under nitrogen flow. After the solution cooled down to room temperature, a solution containing 0.05 mmol $H_2PtCl_6{\cdot}6H_2O$ + 0.05 mmol $Cu(acac)_2$ in 5 ml OAm was added in followed by stirring for 30 min. Then the completely mixed solution was heated to 230 °C and retained for 1 h under a nitrogen flow, followed by centrifugation and washing for several times with hexane to produce the final solid product denoted as Au@PtCu core–alloy shell NPs.

2.3. Synthesis of AuPtCu ternary alloy and PtCu binary alloy NPs

A mixture of 0.05 mmol $HAuCl_4{\cdot}4H_2O$, 0.05 mmol $H_2PtCl_6{\cdot}6H_2O$ and 0.05 mmol $Cu(acac)_2$ was added into OAm (20 ml), heated to 230 °C, retained for one hour under a nitrogen flow and then AuPtCu ternary alloy NPs were obtained by centrifuging and washing with hexane for several times. The synthesis of PtCu alloy NPs used the same conditions described above but without adding $HAuCl_4{\cdot}4H_2O$.

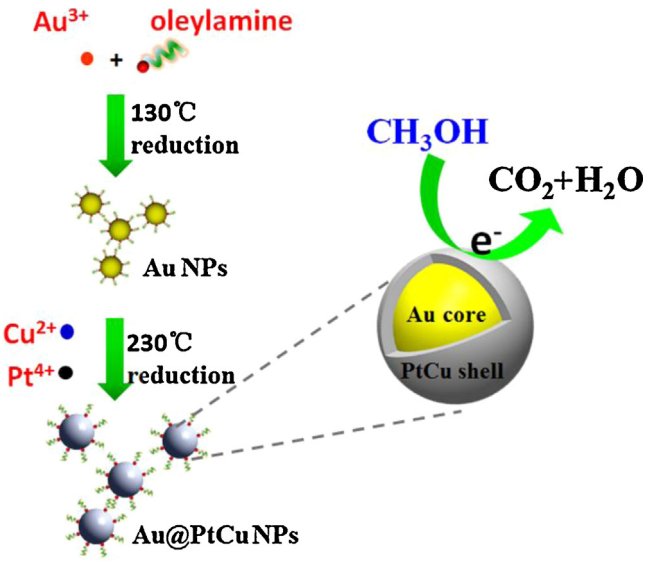

Fig. 1. Scheme of the fabrication process for Au@PtCu core–alloy shell NPs and the catalysis in methanol oxidation reaction.

2.4. Synthesis of Au@PtCu/C, AuPtCu/C and PtCu/C electrocatalysts

The as-prepared Au@PtCu and AuPtCu NPs was added in hexane, respectively, followed by mixing with a pre-sonicated suspension of XC-72 carbon/hexane. The amount of metal loading on XC-72 carbon was adjusted to approximately 40 wt%. After ultrasonication for 2 h, the colloidal mixture was collected by centrifuging and washing with hexane and ethanol for several times.

2.5. Materials characterization

The morphology of prepared NPs was examined by transmission electron microscopy (TEM, JEM-2100) and high angle annular dark field scanning transmission electron microscope (HAADF-STEM) was performed by using Titan G2 60-300 equipped with image corrector and highly sensitive Super-X energy dispersive X-ray (EDX) detector system. Elements composition of the electrocatalysts was analyzed by EDX spectrum equipped on field emission scanning electron microscope (FESEM, JSM7800F). X-ray diffraction (XRD) patterns of prepared electrocatalysts were detected using Shimadzu XRD-7000.

2.6. Electrochemical measurements

The electrochemical experiments were performed with CHI 660D in a three-electrode cell. 5 mg as-prepared catalyst and 50 μL 5 wt% Nafion solution were mixed with 1 mL ethanol, followed by ultrasonically dispersing for about 30 min. To prepare the working electrodes, all catalyst solutions containing a same amount of Pt were pipetted and spread on the surface of glassy carbon electrodes (4 mm diameter, 47.8 $\mu g\,cm^{-2}_{Pt}$). A platinum foil ($1 \times 1\,cm^2$) and a saturated calomel electrode (SCE) were used as the counter and reference electrodes, respectively. The catalytic behaviors of the Au@PtCu/C, AuPtCu/C, PtCu/C, commercial Pt/C and PtRu/C electrocatalysts were characterized by cyclic voltammetry (CV), linear sweep voltammogram (LSV), chronoamperometry (CA) and chronopotentiometry (CP) techniques. Prior to each experiment, the electrodes were cycled in 0.1 M $HClO_4$ solution ranging from −0.22 to 1.1 V at a scan rate of 100 $mV\,s^{-1}$ until a stable voltammogram. CV curves were measured in N_2-satureted 0.1 M $HClO_4$ or/and 0.1 M $HClO_4$ + 0.5 M CH_3OH at a scan rate of 50 $mV\,s^{-1}$. The LSV, CA, and CP curves were conducted in N_2-satureted 0.1 M $HClO_4$ + 0.5 M CH_3OH, respectively.

3. Results and discussion

TEM images in Fig. 2(a–b) show that the as-prepared Au NPs are monodispersed with a uniform size of 6 nm. High resolution TEM (HRTEM) image (inset of Fig. 2b) exhibits a single Au NP with a well-defined crystal structure and fringes with periods of 2.04 and 2.35 Å concurring with the (2 0 0) and (1 1 1) lattice spacing of Au face-centered cubic (fcc), respectively. The TEM image in Fig. 2c shows that Au@PtCu NPs are uniformly distributed with an increased size (8 nm), indicating that the PtCu alloy shell is deposited onto Au core successfully. The formation of small and uniform distributed Au@PtCu NPs could be attributed to the organic solvent OAm, which can efficiently disperse and form complex compounds with the metal ions of a precursor. Furthermore, the metastable compounds can serve as a secondary precursor to be decomposed in a controlled way for tailoring the size and uniformity of the nanoparticles [25]. The distribution of Au, Pt and Cu atoms in the Au@PtCu nanoparticles was evaluated by EDX and HAADF-STEM for more accurate information on the structure and compositional distribution to confirm the core–shell structure [26]. Obviously, the nanoparticles in Fig. 2e depict a darker shell around

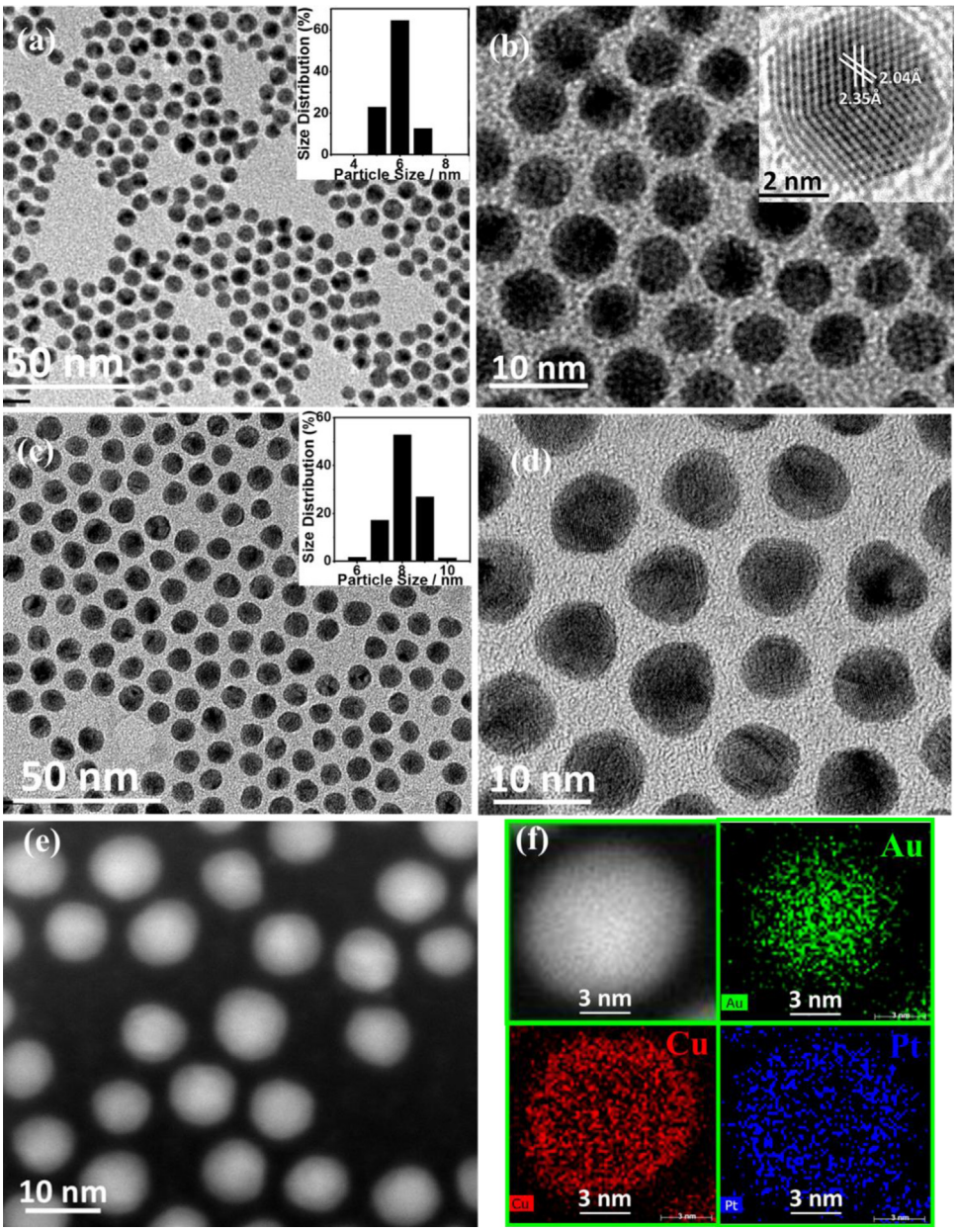

Fig. 2. (a) TEM image of Au NPs with low magnification and the inset is its corresponding size-distribution histogram. (b)TEM image of Au NPs with high magnification and HRTEM of a single Au NP (inset). (c–d) TEM images of Au@PtCu NPs at low and high magnification, respectively. The inset is the corresponding size-distribution histogram of Au@PtCu NPs (c). (e) HAADF-STEM image of prepared Au@PtCu NPs and (f) EDX elemental distribution of Au, Pt and Cu in the representative Au@PtCu NP.

a bright core, and the corresponding STEM-EDX elemental mapping (Fig. 2f) of a representative nanoparticle confirms the formation of Au@PtCu core–alloy shell structure. The composition of Au@PtCu, AuPtCu and PtCu alloy NPs supported on XC-72 carbon was determined by EDX spectrum equipped on FESEM (Fig. S1), respectively. The results reveal that the ratios of Au, Pt and Cu were approximation to that of the reaction mixtures, clearly indicating that the electrocatalyst is formed without loss of any metal precursor.

The crystalline structures of Au@PtCu/C, AuPtCu/C and PtCu/C were investigated by powder XRD. AuPtCu/C exhibits a typical fcc feature (Fig. 3). The wide peak around 25° is ascribed to XC-72 carbon support and other four diffraction peaks at 39.5, 45.8, 67.1 and 80.5° well match with (1 1 1), (2 0 0), (2 2 0) and (3 1 1) facets, respectively. In addition, there is no any impurity peak or monocomponent Au or Cu peak observed, verifying the formation of the AuPtCu ternary alloy. For Au@PtCu/C, the peaks at around 40° can be regards as overlapping of the peak of Au core with PtCu alloy shell peak (Fig. 3 inset), in which a hump of the Au peak can be still observed [27], while the peak of PtCu is right shifted in comparison to the commercial Pt/C, implying that the lattice contraction occurs by Cu incorporated into the Pt fcc structure to form the PtCu alloy phase. The slight right shift of the Au peak positions over the bulk phase is possibly due to the Au core wrapped up by the PtCu shell [28,29]. Thus, the XRD patterns further confirm the core shell structure of Au@PtCu. It is worthy of a note that the weak peak of AuPtCu/C and Au@PtCu/C at about 33° maybe originated from copper oxides.

The electrochemical behaviors of Au@PtCu/C toward methanol oxidation were investigated. For comparison, AuPtCu/C, PtCu/C and commercial Pt/C electrocatalysts were also examined. Since pure Au and Cu catalyst was not active for methanol oxidation reaction, and the addition of Au and Cu can enhance catalytic activity

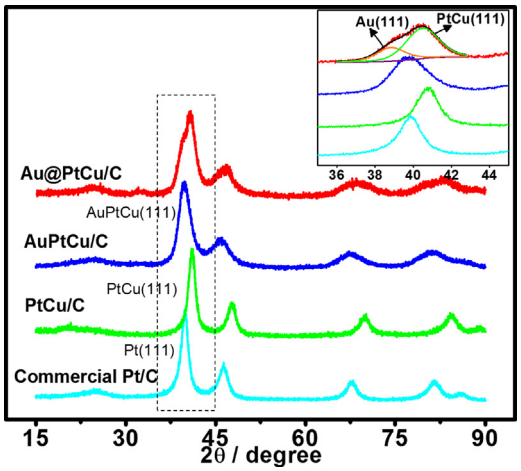

Fig. 3. XRD patterns of Au@PtCu/C, AuPtCu/C, PtCu/C and commercial Pt/C. The inset shows the corresponding enlarged region of the Pt (1 1 1) diffraction peaks.

of Pt, the catalyst activity was evaluated in the base of Pt [30,31]. CV curves in Fig. 4a present the hydrogen adsorption/desorption region from −0.22 to 0.05 V (vs. SCE). The oxidation peaks in more positive potential region can be assigned to the surface metal oxides and the reduction peaks in the negative scans are evidently due to the reduction of the formed oxides. The ECSA is a critical parameter to evaluate the performance of an electrocatalyst since a larger ECSA provides more catalytic active sites [32]. Hydrogen adsorption/desorption region can be used to calculate the ECSA in terms of Eq. (1). [33,34]

$$\mathrm{ECSA} = \frac{\mathrm{Q}}{0.21\mathrm{m\ C cm^{-2}} \times \mathrm{Pt_m}} \quad (1)$$

where Q (mC) and Pt_m are the charge calculated from hydrogen adsorption/desorption region and the integrated Pt loaded on the electrode surface, respectively. 0.21mC cm^{-2} is the charge assuming monolayer adsorption of hydrogen occurs on Pt. The calculated ECSA of Au@PtCu/C is 64.8 $m^2\ g^{-1}{}_{Pt}$, which is remarkably higher than that of AuPtCu/C (38.5 $m^2\ g^{-1}{}_{Pt}$), PtCu/C (31.02 $m^2\ g^{-1}{}_{Pt}$) and commercial Pt/C (25.4 $m^2\ g^{-1}{}_{Pt}$), demonstrating that Au@PtCu/C possesses much more available catalytic active sites. Fig. 4b depicts the methanol oxidation occurred on various Pt-based electrocatalysts in 0.1 M $HClO_4$ + 0.5 M CH_3OH. Typically, the methanol oxidation current peak appears in the positive scan, while the oxidation peak at about 0.45 V during the negative scan is associated with oxidization of the residual carbon species resulted from the positive potential scan [35]. The ratio of the forward oxidation current peak (I_f) to the backward one (I_b) can be considered as an index to evaluate the tolerance of poisoning species such as CO_{ads} and CHO_{ads} [36]. Interestingly, the calculated I_f/I_b ratio of Au@PtCu/C catalyst is 1.48, which is similar to AuPtCu/C (1.46) while higher than that of the PtCu/C (1.31) and commercial Pt/C electrocatalyst (1.27), respectively, suggesting that Au@PtCu/C has much higher electrocatalytic activity toward methanol oxidation and releases relatively less poisoning species than the PtCu/C and commercial Pt/C during the forward scan [36]. Commercial PtRu/C was also investigated for further comparison shown in Fig. 4b. Interestingly, Au@PtCu/C catalyst shows a similar onset potential as the commercial PtRu/C while the peak current of Au@PtCu/C is almost four times higher than that of PtRu/C, indicating that the Au@PtCu/C catalyst provides much higher catalytic performance toward methanol oxidation. To further compare the electrocatalytic activity of the as-prepared catalysts, the peak current was normalized to a specific current density with ECSA and mass current density with the loaded Pt amount (Fig. 4c), respectively. Very impressively, the specific current density of 14.1 A $m^{-2}{}_{Pt}$ for Au@PtCu/C is higher than that of AuPtCu/C (12.1 A $m^{-2}{}_{Pt}$), PtCu/C

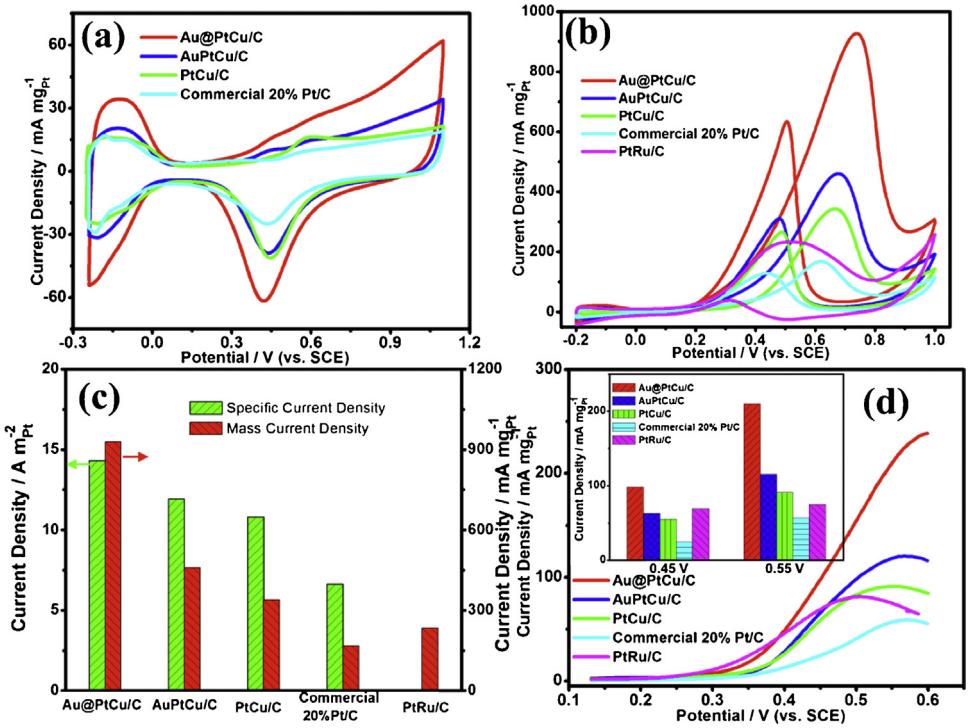

Fig. 4. (a) CV curves of Au@PtCu/C, AuPtCu/C, PtCu/C and commercial Pt/C in N_2-saturated 0.1 M $HClO_4$ (b) CV curves of Au@PtCu/C, AuPtCu/C, PtCu/C, commercial PtRu/C and commercial Pt/C in N_2-saturated 0.1 M $HClO_4$ + 0.5 M CH_3OH. Scan rate: 50 mV s^{-1} (c) The comparison catalytic activity concerning active Pt for Au@PtCu/C, AuPtCu/C, PtCu/C, commercial Pt/C and PtRu/C catalysts at peak potential. The specific activity of commercial PtRu/C is not shown here due to the ECSA of PtRu/C catalyst is hard to calculate from hydrogen adsorption/desorption process. (d) LSV curves of various electrocatalysts and the catalytic activity with regard to active Pt (inset). Scan rate of 5 mV s^{-1}.

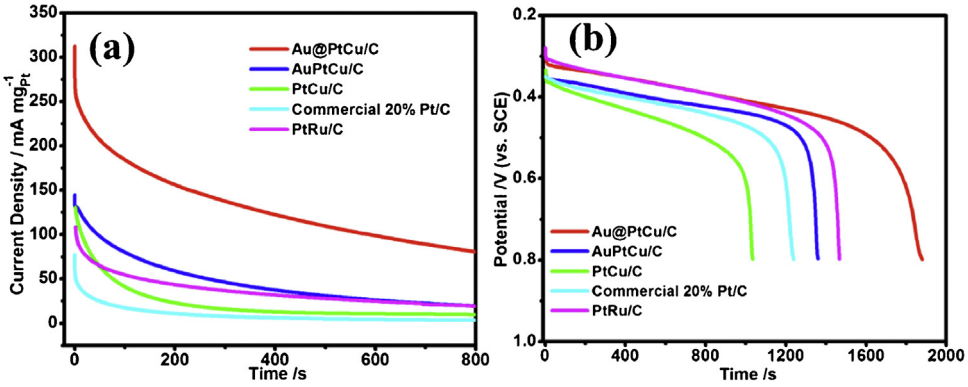

Fig. 5. Chronoamperometry (0.50 V vs. SCE) (a) and chronopotentiometry (8 mA mg^{-1} $_{Pt}$) (b) of Au@PtCu/C, AuPtCu/C, PtCu/C, commercial Pt/C and PtRu/C catalysts in N_2-saturated 0.1 M $HClO_4$ + 0.5 M CH_3OH.

(10.9 A m^{-2}_{Pt}) and commercial Pt/C (6.7 A m^{-2}_{Pt}), respectively, which is consistent with the ratio of I_f/I_b obtained from Fig. 4b. The high performance is generated by modification of the electronic structure between PtCu alloy shell and Au core [13,37]. The Au@PtCu/C catalyst also shows the highest mass current density of up to 927 mA mg^{-1}_{Pt} toward methanol oxidation, which is 2, 2.7, 5.5 and 4 times higher than that of AuPtCu/C (461 mA mg^{-1}_{Pt}), PtCu/C (340 mA mg^{-1}_{Pt}), commercial Pt/C (165 mA mg^{-1}_{Pt}) and PtRu/C (233 mA mg^{-1}_{Pt}), respectively. This could be ascribed to the highest ESCA for more available catalytic active sites. Fig. 4d shows LSV curves at a slow scan rate of 5 mV s^{-1} for various electrocatalysts, and the peak current density of Au@PtCu/C is 238 mA mg^{-1}, which is almost 2, 2.5, 4 and 3 times higher than that of AuPtCu/C (121 mA mg^{-1}), PtCu/C (92.2 mA mg^{-1}), commercial Pt/C (59 mA mg^{-1}_{Pt}) and PtRu/C (80.5 mA mg^{-1}_{Pt}), respectively. This is also in good agreement with the CV result in Fig. 4b. Moreover, the inset of Fig. 4d shows that the Au@PtCu/C catalyst has higher current density at 0.45 and 0.55 V than others catalysts, further confirming that the Au@PtCu/C catalyst possesses the highest catalytic activity.

The operation stability of Au@PtCu/C, AuPtCu/C, PtCu/C, commercial Pt/C and PtRu/C catalysts toward methanol oxidation reaction was evaluated under the same conditions. The chronoamperometry curves in Fig. 5a measured at 0.5 V (vs. SCE) for 800 s show a current density decay from the initial value due to the formation of poisoning species during the oxidation reaction [38]. However, the Au@PtCu/C catalyst has the highest initial current density and retains 80.5 mA mg^{-1}_{Pt} after 800 s, which is much higher than that of AuPtCu/C (19.9 mA mg^{-1}_{Pt}), PtCu/C (9.7 mA mg^{-1}_{Pt}), commercial Pt/C (3.9 mA mg^{-1}_{Pt}) and PtRu/C (20.6 mA mg^{-1}_{Pt}), indicating that the Au@PtCu/C catalyst has much better stability during operation. EDX experimental result (Fig. S2) further indicates that the Au@PtCu nanoparticle can still retain a core–alloy shell structure after the electrochemical analysis. The chronopotentiometric results for the catalysts with a same load of 8 mA mg^{-1}_{Pt} in Fig. 5b exhibit that the polarization potential of the electrode increases gradually at the beginning but jumps to a higher potential later. This is very possibly caused by the poisoning species accumulated on the surface of electrocatalysts, resulting in reduced catalytic activity for the higher polarization potential [39]. Obviously, the Au@PtCu/C catalyst has much higher poisoning tolerance ability than that of AuPtCu/C, PtCu/C and commercial Pt/C while showing a significantly lower onset potential (0.32 V) than that of AuPtCu/C (0.35 V), PtCu/C (0.35 V) and commercial Pt/C(0.36 V). The result also confirms that PtRu/C catalyst has a similar onset potential as that of Au@PtCu/C; however, the later exhibits higher operation stability than the former. The excellent catalytic performance is very likely to be contributed from a synergistic effect of the unique physical core–shell nanostructure and rational chemical metal composition, in which the Au core that improves the electron transfer from Au to Pt while suppressing Pt dissolving and NPs agglomerating in acid medium [40], while Cu could modify the electronic and geometric structures of surface Pt to enhance the catalytic activity toward methanol oxidation and decrease the poisoning species adsorption as observed from other transition-metal-Pt alloys-based catalysts [41].

4. Conclusions

In summary, we use one-pot approach to successively prepare small and uniformly dispersed Au core and PtCu alloy shell NPs as a catalyst for methanol oxidation, demonstrating an ECSA up to 64.8 m^2 g^{-1}_{Pt}, which is about 1.7, 2.1 and 2.5 times higher than that of AuPtCu/C (38.5 m^2 g^{-1}_{Pt}), PtCu/C (31.02 m^2 g^{-1}_{Pt}) and commercial Pt/C (25.4 m^2 g^{-1}_{Pt}), respectively. In comparison to AuPtCu/C, PtCu/C, commercial Pt/C and PtRu/C electrocatalysts, Au@PtCu/C exhibits the highest catalytic activity and the best stability toward methanol oxidation reaction. The remarkable good performance is contributed from a synergistic effect of Au core and PtCu shell with small-sized and uniform dispersion. This work provides a great potential for a new low-Pt loading electrocatalyst to replace expensive commercial Pt/C catalyst for high performance DMFCs.

Author contributions

Zhao Z. L. and Zhang L. Y. contributed equally to this work.

Acknowledgement

We gratefully acknowledge to the financial support from Institute for Clean Energy & Advanced Materials, Faculty of Materials and Energy, Southwest University, Chongqing, P.R. China, Chongqing Key Laboratory for Advanced Materials and Technologies of Clean Energies and Chongqing Science and Technology Commission (cstc2012gjhz90002), P.R. China.

Appendix A. Supplementary data

Supplementary data associated with this article can be found, in the online version, at http://dx.doi.org/10.1016/j.apcatb.2015.03.020.

References

[1] M. Winter, R.J. Brodd, Chem. Rev. 104 (2004) 4245–4270.
[2] H. Liu, C. Song, L. Zhang, J. Zhang, H. Wang, D.P. Wilkinson, J. Power Sources 155 (2006) 95–110.
[3] Y. Qiao, C.M. Li, J. Mater. Chem. 21 (2011) 4027–4036.

[4] M.K. Debe, Nature 486 (2012) 43–51.
[5] C.X. Guo, L.Y. Zhang, J. Miao, J. Zhang, C.M. Li, Adv. Energy Mater. 3 (2013) 167–171.
[6] C. Bianchini, P.K. Shen, Chem. Rev. 109 (2009) 4183–4206.
[7] Y. Wang, X. Wang, C.M. Li, Appl. Catal. B: Environ. 99 (2010) 229–234.
[8] Z. Cui, C.X. Guo, C.M. Li, J. Mater. Chem. A 1 (2013) 6687.
[9] E. Antolini, Energy Environ. Sci. 2 (2009) 915.
[10] H.-H. Li, C.-H. Cui, S. Zhao, H.-B. Yao, M.-R. Gao, F.-J. Fan, S.-H. Yu, Adv. Energy Mater. 2 (2012) 1182–1187.
[11] L. Guo, S. Chen, L. Li, Z. Wei, J. Power Sources 247 (2014) 360–364.
[12] G. Gupta, D.A. Slanac, P. Kumar, J.D. Wiggins-Camacho, X. Wang, S. Swinnea, K.L. More, S. Dai, K.J. Stevenson, K.P. Johnston, Chem. Mater. 21 (2009) 4515–4526.
[13] D. Xu, Z. Liu, H. Yang, Q. Liu, J. Zhang, J. Fang, S. Zou, K. Sun, Angew. Chem. Int. Ed. 48 (2009) 4217–4221.
[14] E. Antolini, J.R.C. Salgado, E.R. Gonzalez, Appl. Catal. B: Environ. 63 (2006) 137–149.
[15] S. Koh, P. Strasser, J. Am. Chem. Soc. 129 (2007) 12624–12625.
[16] E. Antolini, Appl. Catal. B: Environ. 74 (2007) 324–336.
[17] J.X. Wang, H. Inada, L. Wu, Y. Zhu, Y. Choi, P. Liu, W.-P. Zhou, R.R. Adzic, J. Am. Chem. Soc. 131 (2009) 17298–17302.
[18] L.X. Ding, G.R. Li, Z.L. Wang, Z.Q. Liu, H. Liu, Y.X. Tong, Chem. Eur. J. 18 (2012) 8386–8391.
[19] D. Wang, H.L. Xin, R. Hovden, H. Wang, Y. Yu, D.A. Muller, F.J. DiSalvo, H.D. Abruña, Nat. Mater. 12 (2013) 81–87.
[20] J. Zeng, J. Yang, J.Y. Lee, W. Zhou, J. Phys. Chem. B 110 (2006) 24606–24611.
[21] H. Wang, R. Wang, H. Li, Q. Wang, J. Kang, Z. Lei, Int. J. Hydrogen Energy 36 (2011) 839–848.
[22] R. Lin, C. Cao, T. Zhao, Z. Huang, B. Li, A. Wieckowski, J. Ma, J. Power Sources 223 (2013) 190–198.
[23] V. Mazumder, M. Chi, K.L. More, S. Sun, J. Am. Chem. Soc. 132 (2010) 7848–7849.
[24] C. Hsu, C. Huang, Y. Hao, F. Liu, Phys. Chem. Chem. Phys. 14 (2012) 14696–14701.
[25] S. Mourdikoudis, L.M. Liz-Marzaín, Chem. Mater. 25 (2013) 1465–1476.
[26] R. Choi, S.I. Choi, C.H. Choi, K.M. Nam, S.I. Woo, J.T. Park, S.W. Han, Chem. Eur. J. 19 (2013) 8190–8198.
[27] S. Xiao, F. Xiao, Y. Hu, S. Yuan, S. Wang, L. Qian, Y. Liu, Sci. Rep. 4 (2014) 4370.
[28] S. Alayoglu, B. Eichhorn, J. Am. Chem. Soc. 130 (2008) 17479–17486.
[29] A.U. Nilekar, S. Alayoglu, B. Eichhorn, M. Mavrikakis, J. Am. Chem. Soc. 132 (2010) 7418–7428.
[30] H.H. Li, S. Zhao, M. Gong, C.H. Cui, D. He, H.W. Liang, L. Wu, S.H. Yu, Angew. Chem. 52 (2013) 7472–7476.
[31] S. Guo, S. Zhang, X. Sun, S. Sun, J. Am. Chem. Soc. 133 (2011) 15354–15357.
[32] H. Zhao, J. Yang, L. Wang, C. Tian, B. Jiang, H. Fu, Chem. Commun. 47 (2011) 2014–2016.
[33] B. Lim, M. Jiang, P.H. Camargo, E.C. Cho, J. Tao, X. Lu, Y. Zhu, Y. Xia, Science 324 (2009) 1302–1305.
[34] L.Y. Zhang, C.X. Guo, Z. Cui, J. Guo, Z. Dong, C.M. Li, Chem. Eur. J. 18 (2012) 15693–15698.
[35] T. Iwasita, Electrochim. Acta 47 (2002) 3663–3674.
[36] L. Feng, G. Gao, P. Huang, X. Wang, C. Zhang, J. Zhang, S. Guo, D. Cui, Nanoscale Res. Lett. 6 (2011) 1–10.
[37] S. Wang, X. Wang, S.P. Jiang, Phys. Chem. Chem. Phys. 13 (2011) 6883–6891.
[38] S. Wang, S.P. Jiang, T. White, J. Guo, X. Wang, J. Phys. Chem. C 113 (2009) 18935–18945.
[39] Z. Zhao, X. Fang, Y. Li, Y. Wang, P.K. Shen, F. Xie, X. Zhang, Electrochem. Commun. 11 (2009) 290–293.
[40] J. Zhang, K. Sasaki, E. Sutter, R.R. Adzic, Science 315 (2007) 220–222.
[41] H. Yang, J. Zhang, K. Sun, S. Zou, J. Fang, Angew. Chem. Int. Ed. 49 (2010) 6848–6851.